Lawrence Berkeley National Laboratory
LBL Publications

Title
New Developments in Dilute Nitride Semiconductor Research

Permalink
https://escholarship.org/uc/item/85t4q42h

Authors
Shan, W.
Walukiewicz, W.
Yu, K.M.
et al.

Publication Date
2006

eScholarship.org Powered by the California Digital Library
University of California

CHAPTER 17

NEW DEVELOPMENTS IN DILUTE NITRIDE SEMICONDUCTOR RESEARCH

W. Shan[1], W. Walukiewicz[1], K.M. Yu[1], J. Wu[2], J.W. Ager III[1], and E.E. Haller[1,3]

1. *Materials Sciences Division, Lawrence Berkeley National Laboratory, Berkeley, CA 94720*

2. *Department of Chemistry and Chemical Biology, Harvard University, Cambridge, MA 02138*

3. *Department of Materials Science and Engineering, University of California, Berkeley, CA 94720*

1. Introduction

Dilute nitrides, especially $GaAs_{1-x}N_x$ and $Ga_{1-y}In_yAs_{1-x}N_x$, have attracted recently considerable attention from both scientific and technological perspectives. The advances in thin-film deposition technology have allowed these materials to be grown with ever-improving crystalline quality, which in turn improves their optical properties and electronic performance. This enables the fundamental study of the unusual properties of these materials. These include a reduction of the fundamental band-gap energy,[1,2] a significant increase in electron effective mass and a decrease in electron mobility.[3-5] Furthermore, a new optical transition (E_+) above the fundamental band gap energy has been observed.[6,7] Most notable is the large observed band-gap bowing. The incorporation of only one percent nitrogen into GaAs induces a strikingly large reduction of 0.18 eV in the fundamental band-gap energy.[8] The mechanism by which the addition of nitrogen changes the properties of these III-N-V materials appears to be fundamentally different from that in other III-V alloy systems such as $Al_xGa_{1-x}As$. This creates new opportunities for band-gap engineering and optoelectronic device-structure designs with the direct band gaps of these dilute-nitride alloys accessible to the near-IR, which is of great importance for telecommunications and solar power conversion applications.

2. Material Properties

The novel material properties of dilute nitrides were first discovered in the early 1990's. In the quest to close the gap between the nitrides and arsenides thus to achieve the goal of fabricating light emitting devices covering the entire visible spectral region, Weyers and coworkers succeeded in growing GaN_xAs_{1-x} alloys using plasma assisted metalorganic chemical vapor deposition (MOCVD).[1] To their surprise, they found that these alloys exhibit a considerable red shift in photoluminescence and absorption edge rather than the anticipated blue shift. Furthermore, application of simple interpolation between the properties of the end point materials using first or second order polynomials within the virtual crystal approximation (VCA), in which the random alloy potential is approximated by a periodic lattice of average atomic potential[9-11] and has the trend of increasing band-gap energy with decreasing lattice constant, led to large and composition dependent bowing parameters[12-15] beyond common experience.

The uncommon physical properties are the consequence of the extraordinary chemical characteristics of nitrogen compared to other group–V elements. These chemical characteristics, in turn, cause difficulties in incorporating nitrogen in III–V semiconductor crystals to form randomly mixed III-N-V nitride alloys. The conventional non-nitride III-V compound semiconductors do not easily crystallize in the wurtzite form, the crystal structure of GaN. It is therefore expected that GaNAs and the other analogous alloys will crystallize in the zinc-blende structure. There is a large miscibility gap that makes it difficult to prepare the alloys with large N fractions. At present, growth of III–N–V alloys is still considered challenging and bulk crystals have not been grown. To date most reports on III–N–V alloys involve thin films grown by molecular beam epitaxy (MBE) using RF plasma nitrogen radical beam source or metalorganic chemical vapor deposition (MOCVD) with dimethylhydrazine as nitrogen source.[16] The nitrogen contents in such samples were usually determined using secondary ion mass spectrometry (SIMS) and indirectly from the change of the lattice constant measured with the (004) reflection in double-crystal x-ray diffraction.

One of the major challenges for the growth of dilute nitrides is the completely different set of boundary conditions that affect the choice of the epitaxial growth technique. Both MBE and MOCVD have been used to grow dilute nitride materials, however, the issues governing choice are

appreciably more complex and challenging than for GaAs-based and InP-based alloy systems that are extensively used in optoelectronic applications. The situation for growth of GaNAs and GaInNAs is entirely different compared to the InGaAsP materials systems. First of all, in order to incorporate sufficient N, the growth has to occur at much lower growth temperatures and under metastable growth conditions within the miscibility gap region of the GaInNAs alloy. This is due to the different basic crystal structures of the constituent alloys and their regions of growth compatibility: GaN is a hexagonal (wurtzite) crystal grown at relatively high temperatures while GaAs is cubic (zinc-blende) grown at significantly lower temperatures, creating a miscibility gap in the alloys.[17] Hence, as either or both N and growth temperature increase, phase segregation occurs.

Kondow and coworkers used an N plasma source added to a gas source MBE system.[18] This growth technique provided material which showed the potential for GaInNAs. However, issues related to H incorporation and strong growth temperature composition sensitivity due to the low arsine cracking efficiency set limitations, particularly for large scale deposition using this approach. Solid-source MBE with an atomic N plasma source has proven to be the most versatile system to allow growth at the lowest temperatures and over the largest range of N and In compositions.[17] The single most critical parameter controlling growth is the growth temperature. When the growth temperature exceeds a critical value, MBE growth begins to change from 2D, layer-by-layer growth to 3D island growth with microphase segregation.[17] There is a N composition dependence on suitable growth temperature, however, $420^{o}C < T < 450^{o}C$ maintains 2D epitaxial growth over the greatest range of N compositions. The V/III supply ratio also has an impact on growth, but much less so than temperature.

Because growth must occur at much lower temperatures, MOCVD growth is far more challenging than MBE growth. Compared to MOCVD growth of N-based wide-band-gap systems, which use ammonia as the N source, the growth temperature for GaInNAs is too low to achieve reasonable cracking of either ammonia or arsine. Need to use new sources with complex precursor reactions and highly nonlinear incorporation ratios greatly complicate the growth compared to conventional III–V materials systems. The higher growth temperatures limit the N incorporation where micro-phase segregation begins and

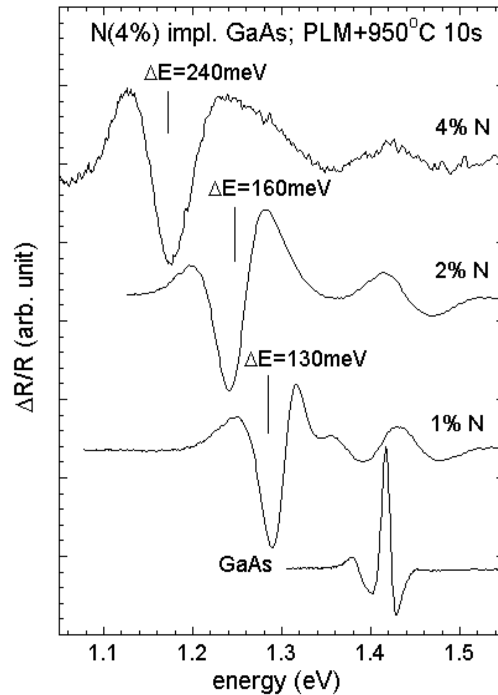

Figure 1. PR spectra measured from a series of samples implanted with increasing amounts of N (x_{imp}) and processed by PLM at an energy fluence of 0.34J/cm^2 and subsequent RTA at 950ºC for 10 sec.

makes it extremely challenging to reach the N compositions needed to achieve 0.8-1.0 eV band gap.[19]

A new method for synthesizing dilute nitrides was developed during recent years. Nitrogen implantation followed by rapid thermal annealing (RTA) was found to be a practical and convenient method for the formation of diluted III-N-V alloys.[20,21] The fundamental band-gap energies for the ion beam synthesized thin films of GaN_xAs_{1-x}, InN_xP_{1-x} and $Al_yGa_{1-y}N_xAs_{1-x}$ obtained by N^+ implantation into GaAs, InP and $Al_yGa_{1-y}As$ were found to decrease with increasing N implantation dose in a manner similar to that observed in epitaxially grown thin films. In GaN_xAs_{1-x} the highest value of x achieved using N^+-implantation and

conventional RTA technique was 0.006 corresponding to an N activation efficiency of ~15%. In the course of optimizing the annealing conditions in these studies, it was found that, in GaNAs formed in this way, the substitutional N_{As} is thermally unstable at temperatures higher than 850°C and will precipitate to form N_2 filled voids.[22]

More recently, it has been shown that pulsed laser melting (PLM) of N-implanted III-Vs dramatically improves the incorporation of N on the group-V element site.[23,24] In PLM, the near surface absorption of a single intense laser pulse instantaneously melts the implant-damaged or amorphized layer. This is followed immediately by rapid epitaxial regrowth from the liquid. Epitaxy is seeded at the solid-liquid interface by the crystalline bulk in a manner very similar to liquid phase epitaxy (LPE) but with the whole process occurring on a much shorter time scale, typically between 10^{-8}-10^{-6} second.[25,26] Figure 1 shows a series of photoreflectance (PR) spectra from GaAs implanted with increasing amounts of N processed by PLM with an energy fluence of 0.34 J/cm^2 and subsequently by RTA at 950ºC for ten seconds. Such PLM-RTA post-implantation treatments appear to represent the "optimum" process conditions found to date and the samples so formed have clear, sharp optical transitions. The amount of N incorporated in the As sublattice ("active" N) for the GaN_xAs_{1-x} layers formed by this method can be estimated using the BAC model and is ~40-60% of the implanted value. This is over five times higher than the activation efficiency observed in samples processed by RTA only.[21] Such a drastic improvement can be attributed to the extremely short melt duration (~2×10^{-7} s) and re-growth process that promotes N substitution in the As site and inhibits the formation of nitrogen voids.[24] In addition to the enhanced N incorporation, the dilute nitride layers synthesized by N^+-implantation followed by PLM-RTA were also found to be thermally stable up to annealing temperature > 950°C. This improved sample synthesis technique provides a convenient and reliable method, in addition to conventional epitaxial growth techniques,[2,4,12] for preparing large variety of dilute nitride samples.

3. Device Applications

3.1 *Long-wavelength Laser Diodes for Telecommunications*

The rapid growth of the internet and data transmission in recent years has driven the bandwidth of optical fiber networks, particularly in the areas

of metro area networks (MAN) and local area networks (LAN), to be continuously expanded to meet the ever increased demand. Low cost, single mode vertical cavity surface-emitting lasers (VCSELs) operating in longer wavelengths and at room temperature are an essential element for data communications in a gigabit MAN or LAN architecture because the most used GaAs-based 850-nm VCSELs for data communications suffers a severe drop in transmission distance as the bit-rate increases. Although InGaAsP/InP has long been the materials system for distributed feedback (DFB) edge-emitting lasers that have been the sources for long-haul, 1.55 μm optical-fiber backbone networks over the years, the inherent material problem of insufficient refractive index contrast, makes it impossible to meet the requirements for distributed Bragg reflector quarter-wave VCSEL mirrors, particularly in 1.3 μm. It is also not feasible to use such expensive DFB lasers for data communications in MAN and LAN that would require millions of them.

In addition, use of Raman amplifiers in the dense-wavelength division-multiplexing architectures within the S- and L-bands require high-power pump lasers similar to 0.98 μm strained InGaAs/GaAs QWs lasers, but at longer wavelengths (1.2 – 1.5 μm). The well-known materials limitations of the InGaAsP system make it nearly impossible for applications in long wavelength high-power pumping lasers. The small heterojunction conduction-band offset between InP and InGaAsP (~40% ΔE_g) limits electron confinement in the QWs, resulting in a much lower characteristic temperature T_0 compared to the InGaAs/GaAs materials used for EDFA pumps.

Since the bandgap energy decreases for decreasing lattice constant in mixed group-V dilute nitrides, they can dramatically expand the range of applications of III–V alloy semiconductors and significantly increase freedom in designing semiconductor devices. Therefore, there are possibilities in which novel devices can be created or the performance of current devices can be drastically improved. It is Kondow and his coworkers who first proposed GaInNAs as an alternative active-region material for semiconductor laser diodes operating in the 1.3 μm and 1.55 μm regions, the telecommunications windows of optical fibers.[18] It is possible to make devices with significantly superior performance than the ones based on the InGaAsP/InP materials system due to the unusual physical properties of the dilute nitride alloy semiconductors: Adding In to GaAs increases the lattice constant of InGaAs alloys, whereas adding N to GaAs decreases the lattice constant of GaNAs alloys. Therefore

GaInNAs can be grown lattice-matched or pseudomorphically nearly-matched on a GaAs substrate. Both In and N have the effect of reducing the band-gap energy that makes GaInNAs suitable for long-wavelength laser diodes (1.3–1.55 μm and longer wavelengths). Furthermore, as will be discussed in the next section, incorporating of N into GaAs has a negligible effect on the valence band so that almost the entire change in the band gap between GaNAs and GaAs is accommodated by the conduction-band offset alone. All these unusual properties make GaInNAs one of the most attractive new materials for both VCSELs and high-power edge-emitting laser applications.

By combining GaInNAs with GaAs or other wide-gap materials that can be grown on a GaAs substrate, a type-I band lineup is achieved and, thus, very deep quantum wells can be fabricated, especially in the conduction band.[16] Since the electron overflow from the wells to the barrier layers at high temperatures can be suppressed, GaInNAs is highly attractive for overcoming the poor temperature characteristics of conventional InGaAsP/InP long-wavelength laser diodes.

In the case of VCSELs, GaInNAs can utilize structures almost identical to 850 nm VCSELs that are now in large-scale production. In order to greatly expand broadband amplifier used in MANs, the key features that must be achieved are sufficient power and low cost. At this point it is clearly far from obvious that this new material will reach the leading position for the development of a broad range of VCSELs and edge-emitting lasers that will be the foundation of lower cost fiber optical networks for telecommunication.

3.2 *Solar Cells for Photovoltaic Solar Power Conversion*

High-efficiency GaInP/GaAs/Ge monolithic series-connected three-junction solar cells are currently in production for space applications and are the leading candidates for terrestrial concentrator applications.[27-29] However, the next generation of four-junction devices with considerably higher efficiencies require a set of III–V materials with a band gap energy lower than that of GaAs but higher than that of Ge, preferably lattice matched to GaAs to minimize strain-induced defects that severely degrade solar cell performance.[30] The discovery by Weyers *et al.* of the anomalously large band-gap reduction in GaNAs[1] and the introduction of GaInNAs as a 1 eV semiconductor, lattice matched to GaAs for laser applications by Kondow *et al.*[18] has quickly led to the realization that

GaInNAs could be also a suitable material for next-generation solar cell designs.

A solar cell must convert photons to electron–hole pairs and separate them into electrons and holes. The voltage of a solar cell is limited by the lowest band-gap energy of the semiconductor. The absorption coefficient $\alpha(E)$ of a given semiconductor material is a measure of how strongly a photon with a particular wavelength will interact with the semiconductor, and is inversely proportional to the distance within which the photon will most likely be absorbed. Both the thickness of a solar cell and its carrier collection length (i.e., its combined diffusion length and depletion width) must be greater than $1/\alpha(E)$ in order to collect a significant fraction of photons of a particular wavelength. Only strongly absorbing direct-gap semiconductors are useful in thin-film solar cells. In a typical solar cell, electrons and holes are separated by the electric field generated by the diffusion potential of a p–n junction. In high-quality semiconductors, these carriers can also diffuse through a field-free region to the p–n junction, allowing collection from relatively thick layers of semiconductor.

The currently most advanced and complicated 1.8 eV GaInP/1.4 eV GaAs/1.0 eV GaInNAs/0.7 eV Ge lattice matched four-junction structure has the potential for extremely high efficiencies.[30] The novel component of this structure is the 1 eV GaInNAs third junction. Single-junction 1.0 eV GaInNAs cells lattice matched to GaAs have been studied most extensively.[31-37] For a 1.0 eV solar cell to be current-matched in the four-junction devices described above, nearly unity internal quantum efficiencies (QE) are required in the energy range 1.0–1.4 eV. Unfortunately, internal QEs of actual devices have reached only about 70% because of poor minority-carrier diffusion lengths. These 70% QEs were achieved by using non-standard designs to minimize the effects of poor diffusion lengths, such as designs using p–i–n type structures with regions of low carrier concentration[31,33] or designs using annealed thick n-type emitter layers.[34] In contrast, p–n junction designs using a thin highly doped ($\sim 1\times10^{18}$ cm^{-3}) emitter and a thicker moderately doped ($\sim 1 \times10^{17}$ cm^{-3}) base, a design which works well for GaAs cells, typically result in <25% internal QE because of the low GaInNAs diffusion length.[31] The cause for short diffusion lengths of minority carriers is a combined effect of low mobilities and short lifetimes that are still not fully understood. Further improvement on the material quality is

inevitably needed in order to achieve nearly unity internal quantum efficiency.

4. Origin of Band-gap Reduction in Dilute Nitrides

4.1 *Large Band-gap Bowing and Early Impurity Models*

The unexpectedly strong effect of the introduction of N in III-V compound semiconductors on the fundamental band gap is related to the fact that replacement of atoms such as As with the much smaller and more electronegative N atom leads to a large, local perturbation of the crystal lattice potential. The electronegativity of N is 3.00, while that of P, As, or Sb is in a range from 2.2 to 1.8.[38] Although it has been known for a long time that small quantities of nitrogen form deep, localized impurity states in GaAs and GaP, the unexpected discovery of a considerable red shift in photoluminescence and absorption edge rather than the expected blue shift, together with a giant bowing parameter, in the GaNAs alloy was a surprise to many.

An early theoretical study predicted a bowing parameter C=25 eV for the direct energy gap ($E_g=A+Bx+Cx^2$) of GaNAs.[39] C=18 eV was obtained from PL measurements of GaNAs with N concentration less than 1.5%.[13] The same result was inferred from studies of the GaNAs near the two binary limits, with the decrease in the energy gap being linear for N fractions as high as 3%.[40] A quadratic form with C=11 eV fit the results of an ellipsometry study for x=3.3% fairly well.[41] Other studies of dilute GaNAs indicated bowing parameters as large as 22 eV.[42-44] A series of first-principles calculations examined various aspects of the band structure for GaNAs, including ordering effects.[45-50] Those studies found that the band-edge wave functions in GaNAs tend to be localized impurity-like states, with the conduction-band wave function strongly localized on the As sublattice and the valence-band wave function on the N sublattice. In order to avoid the early semimetallic transition predicted by using C=20 eV, Uesugi *et al.* proposed a more gradual reduction of the bowing parameter with composition, and attributed the discrepancy to different strain conditions in the different studies.[8]

4.2 *Band Anticrossing*

It is well known that an isolated N atom introduces a localized state with energy level E_N in conventional III-V materials. In most cases, this level is located very close to the conduction band edge. It lies at about 0.25 eV above the conduction band edge in GaAs and less than 0.1 eV below the conduction band edge in GaP. The existence of such states has been predicted by theoretical calculations within the tight binding approximation framework,[51] and confirmed by experimental measurements under hydrostatic pressure.[52,53] As expected for a localized state the energy level of N shows pressure dependence much weaker than that of the conduction band edge of GaAs. The level was also found to move into the band gap when GaAs is alloyed with AlAs.[54] The highly localized nature of the N states suggests that there is only weak hybridization between the orbits of N atoms and the extended states, $E_M(k)$, of the semiconductor matrix. The electronic band structure of the host crystal is not significantly affected by these low nitrogen concentrations.

However, alloying a few atomic percentage of nitrogen into III-V compounds drastically modifies the electronic band structure. A pressure dependent study[6] found that all the $Ga_{1-x}In_xN_yAs_{1-y}$ samples exhibit a much weaker dependence of the band gap energy at low pressures, and a tendency of the energy gap to saturate at high pressures. The saturation is clearly visible in the samples with lower N contents. The pronounced change in the pressure dependence of the energy gap can only be understood in terms of a pressure-induced transformation of the nature of the lowest conduction band states, namely from extended to highly localized. The gradual nature of the transformation cannot be associated with a pressure-induced crossover of non-interacting Γ and X conduction-band valleys but rather suggests that it is a manifestation of an anticrossing behavior of two strongly interacting energy levels with distinctly different pressure dependencies. In order to explain the observed pressure dependence, a simple band anticrossing (BAC) model of two interacting energy levels; one associated with extended states of the GaInAs matrix and the other with the localized N states, was proposed to explain the large changes in the band structure of the resulting dilute III-N-V nitrides. By assuming that N atoms are randomly distributed over the group V sites and are only weakly coupled to the extended states of the conduction band of the host semiconductor matrix, the dispersion relations of the two interacting bands takes the form[6]

$$E_{\pm}(k) = \frac{1}{2}\left\{ \left(E_M(k) + E_N\right) \pm \sqrt{\left(E_M(k) - E_N\right)^2 + 4V_{MN}^{\ 2}} \right\}. \qquad (1)$$

Where $E_M(k)$ and E_N are the energies of the unperturbed conduction band and of the localized N state relative to the top of the valence band, respectively. The matrix element $V_{MN}=C_{MN}x^{1/2}$, where C_{MN} is a constant describing the coupling between localized states and the extended conduction-band states and x is the alloy composition. A very important inference of this model is that it predicts that the interaction of the conduction-band edge with the dispersionless N level results in a splitting of the conduction band into two highly nonparabolic subbands, $E_-(k)$ and $E_+(k)$. The energy positions of the subband edges E_- and E_+

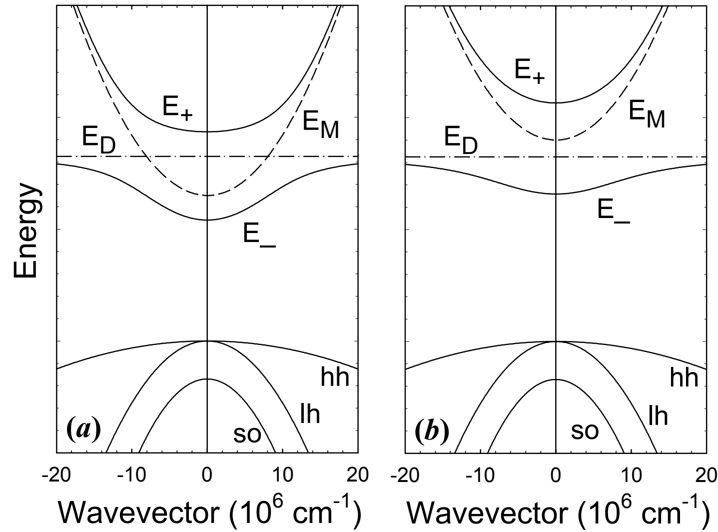

Figure 2. Illustration of the effects of band anticrossing on the conduction band structure in the vicinity of Γ-point minimum. (a) The N induced localized state resonant with the conduction band; (b) The localized state located below the conduction band. The solid lines are the restructured E_- and E_+ subbands resulting from the band anticrossing interaction between the localized states (dash-dotted line) and the extended states of the conduction band (broken line).

given by Eq.(1) depend on alloy concentration x and the coupling parameter C_{MN}, as well as the location of E_N with respect to the conduction band edge E_M. Although the density-functional calculation of Jones *et al.* also predicted a reduced pressure dependence,[55] the formation of $E_+(k)$ subband is a definitive result of band anticrossing.

Figure 2 shows schematic examples of the calculated band structure based on the BAC model. The interaction between the localized isoelectronic states and the extended conduction-band states has a pronounced effect on the dispersion relation of the two conduction subbands $E_$ and E_+. The effect of the interaction is most pronounced for the states located close to E_N.[56] If the localized state is located within the conduction band of the matrix, as depicted in Fig.2(a), the conduction-band states at the $E_$ edge retain mostly the extended E_M-like character and those at the E_+ edge have a more localized and E_N-like character. The lower conduction subband narrows drastically as the E_N level moves below the bottom of the conduction band. The narrowing of the band leads to a highly nonparabolic dispersion relationship and to a large enhancement of the effective mass and the density of states If the localized state is located below the conduction-band edge then as illustrated in Fig.2(b), the $E_$ subband states become more localized wheras E_+ subband states acquire more of the extended state character. The conduction band dispersion relations predicted by BAC model have been recently confirmed in an elegant magnetotunneling experiment.[57]

Recent theoretical considerations using the tight binding approximation have provided additional refinements for the BAC model.[58-60] The BAC model can be extended to treat ten bands (spin-doubled conduction, valence, and nitrogen impurity bands) by modifying the 8-band ***k·p*** theory to include two extra spin-degenerate nitrogen states to describe the electronic band structure of GaNAs/GaAs and related heterostructures.[58-62] It was also argued that the electronic structure of GaNAs alloys is determined by interactions between nitrogen, X, L and Γ states[63,64] This provided more parameters to afford greater flexibility in fitting the experimental data. Although the BAC model does not consider anything more complicated than an interaction of randomly distributed localized nitrogen states with the extended states of the conduction band it properly describes all the main characteristics of the electronic structure of dilute nitrides. It ignores possible complex behavior of nitrogen in the semiconductor matrix, e.g., the formation of nitrogen pairs and clusters. Detailed studies on the nearest-neighbor

environment of the substitutional N atoms in GaInNAs have shown that the fundamental band-gap energy in quaternary dilute nitride alloys is fairly sensitive to the local environmental conditions especially in the case of quantum well structures.[65,66] A more complicated modeling of the electronic structure based on pseudopotentials[67,68] requires a substantial computational effort. The numerical results are difficult to use. This is why simple band anticrossing has been a method of choice in the design of GaInNAs based optoelectronic devices[69] The recent work by Lindsay *et al.* points out that the most amply verified prediction of the BAC model, the dependence of the band gap on the N content, is be unaffected by the multiplicity of higher-lying states.[70]

4.3 E_- *and* E_+ *transitions*

The downward shift of the E_ transition relative to the top of the valence band represents the fundamental band-gap reduction in dilute nitrides. It has a nonlinear dependence on the N concentration. Figure 3 shows that

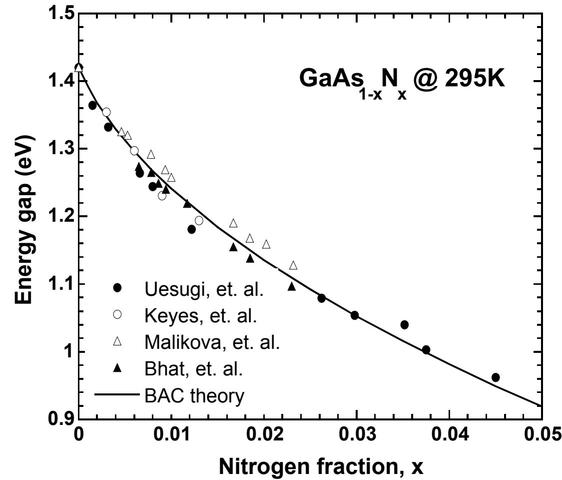

Figure 3. Comparison between the experimentally observed and calculated band-gap reduction of GaN_xAs_{1-x} as a function of N concentration. The calculations are based on the BAC model with C_{MN}=2.7 eV, E_M=1.42 eV, and E_N=1.65 eV.

BAC model with a single fitting parameter C_{MN} provides a very good agreement with the experimental data reported by a number of research groups.[8,71-73] The coupling parameter C_{MN}=2.7 eV was obtained from the fitting of Eq. (1) to the experimentally determined pressure dependence of the band gap of GaN_xAs_{1-x}.[6,74]

The conduction band splitting into two nonparabolic subbands with energy minima at $E_$ and E_+ has been unambiguously observed in GaN_xAs_{1-x} and $Ga_{1-y}In_yN_xAs_{1-x}$ by various groups using a variety of methods.[6,7,75,76] Shown in Fig. 4 are PR spectra recorded with MOCVD-grown GaN_xAs_{1-x} samples. For N containing samples, in addition to the PR spectral features related to the transition across the fundamental band gap ($E_$ transition) and the transition from the top of the spin-orbit split-off valence band to the bottom of the conduction band ($E_+\Delta_0$ transition) as displayed on the PR curve of GaAs, an extra feature (E_+) appears at higher energies in the PR spectra. With increasing N concentration, the $E_$ and $E_+\Delta_0$ transitions shift to lower energy and the E_+ transition moves in the opposite direction toward higher energy[74]

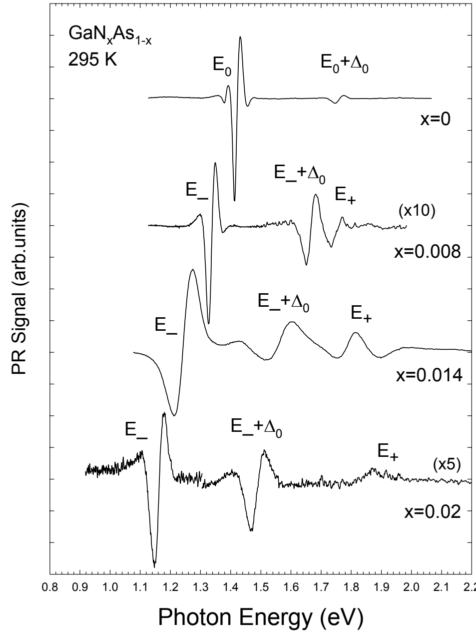

Figure 4. PR spectra of GaN_xAs_{1-x} samples with different N concentrations.

The predictions of the BAC model were further verified by the measurement of the E_- and E_+ transitions under applied pressure.[6,74] The effect of hydrostatic pressure on the optical transitions associated with the E_- and E_+ subband edges in a $GaN_{0.015}As_{0.985}$ sample and a $Ga_{0.95}In_{0.05}N_{0.012}As_{0.988}$ sample is shown in Fig.5. Application of hydrostatic pressure shifts the bottom of the conduction band above the localized N level, gradually changing the character of the E_--subband edge from extended E_M-like to localized E_N-like, and the character of the E_+-subband edge from the localized-like to extended-like. Such a transformation is exactly what the BAC model predicted, schematically depicted in Fig.2. The dispersion relations of the $E_-(k)$ and $E_+(k)$

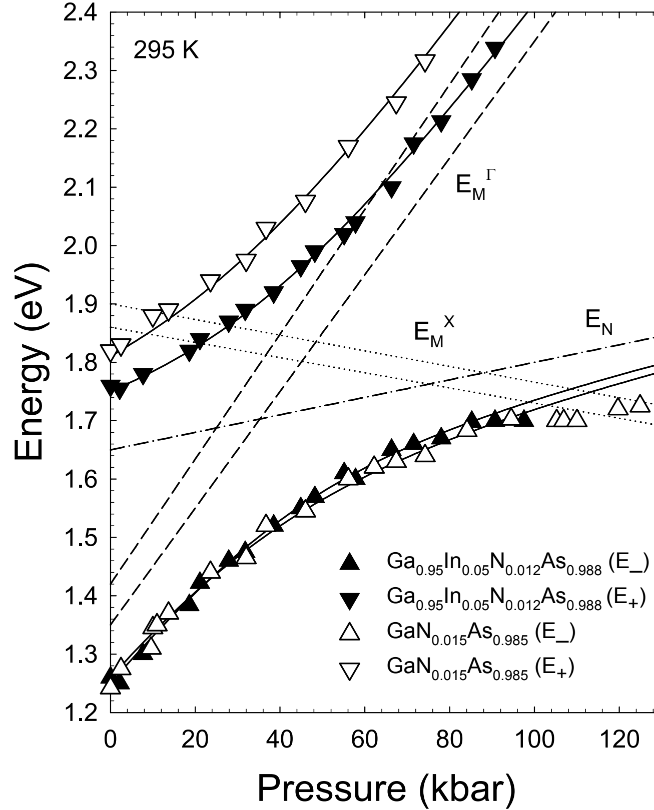

Figure 5. Effects of pressure on the optical transitions associated with the E_- and E_+ transitions in $GaN_{0.015}As_{0.985}$ and $Ga_{0.95}In_{0.05}N_{0.012}As_{0.988}$.

conduction subbands shown in Fig.2(a) represent the case at low pressures where the bottom of the conduction band of the host matrix (E_M) is below the E_N level. Fig.2(b) represents the case at high pressures where E_M is shifted to above the E_N level. The anti-crossing behavior of two strongly interacting energy levels with distinctly different pressure dependencies is unmistakably observed. The E_- transition has a strong dependence at low pressures and gradually saturates at high pressures, whereas the E_+ transition has a weak dependence upon pressure at low pressures and displays a much stronger dependence at high pressures. The solid lines through the experimental data in the figure are the results of calculations using Eq.(1). The best fits to the data yield the energy of the nitrogen state, $E_N = E_V + 1.65$ eV for both samples at atmospheric pressure, and it is independent of In concentration.[6,74] These results prove that the effects of alloying with In on the band gap can be separated from the shifts produced by the interaction with N states, allowing for an independent determination of E_M from a given In concentration in $Ga_{1-y}In_yN_xAs_{1-x}$ alloys.

4.4 *Enhancement in Maximum Free Electron Concentration*

As has been discussed above, the BAC model not only explains the band gap reduction in dilute III-N-V nitrides but it also predicts that the N-induced modifications of the conduction band will have profound effects on the transport properties of those material systems.[57] In particular, the downward shift of the conduction band edge and the enhancement of the DOS effective mass will lead to much enhanced maximum free electron concentration $n_{\max}$.

The electron effective mass as a function of energy can be calculated using the standard definition of the density of states effective mass,

$$m_-^*(\mathbf{k}_F) = \hbar^2 \left| \frac{k}{dE_-(\mathbf{k})/dk} \right|_{k=\mathbf{k}_F} = m_0^* \cdot \left[1 + \frac{{C_{MN}}^2 x}{(E_N - E_-(\mathbf{k}_F))^2} \right]. \quad (2)$$

Where m_0* is the effective mass of the semiconductor matrix and E is the energy in the lower or upper subband measured from the valence band edge. It is seen from Eq.(2) that the effective mass diverges for the electron energy approaching E_N. This is a result of the increasing contribution of the localized N states to the electron states in the lower and upper subbands.

The maximum achievable electron and/or hole concentration is of great importance in semiconductor devices engineering. A universal rule that governs the maximum free carrier concentration achievable by doping has been developed based on an amphoteric native defect model and demonstrated to be valid for a wide variety of semiconductor materials.[77,78] In that model, the type and concentrations of the defects compensating intentionally introduced dopants depends on the location of the Fermi level relative to a material-independent common energy reference called Fermi level stabilization energy E_{FS}. GaAs is predicted, for example, to exhibit limitations on the maximum free electron concentration. Indeed, the maximum electron concentration n_{max} in GaAs achievable under equilibrium conditions has been experimentally confirmed to be limited to about 10^{18}-10^{19}cm^{-3}.[79]

Shown in Fig. 6 are the free electron concentrations in Se doped MOCVD-grown $Ga_{1-3x}In_{3x}N_xAs_{1-x}$ films with x=0 to 0.033 measured by Hall effect and the electrochemical capacitance-voltage (ECV) technique.[80] Since the Se atomic concentrations in these films are at least an order of magnitude higher than the free electron concentration (in the range of $2\sim7\times10^{20}$cm^{-3}), the measured free electron concentration should be regarded as the maximum achievable free electron concentration, n_{max}. The result shown in Fig. 6 indicates that the n_{max} increases strongly with the N concentration. A maximum value of 7×10^{19} cm^{-3} was observed for x=0.033. This value is ~ 20 times that found in a GaAs film (3.5×10^{18} cm^{-3}) grown under the same conditions. The much-enhanced n_{max} in $Ga_{1-3x}In_{3x}N_xAs_{1-x}$ films can be explained by considering the conduction band modifications by N-induced anticrossing interaction. Since the maximum free electron concentration is determined by the Fermi energy with respect to E_{FS}[79] and because the position of the valence band in GaInNAs is independent of N concentration, the downward shift of the conduction band edge toward E_{FS} and the enhancement of the DOS effective mass in GaInNAs leads to a much larger concentration of uncompensated, electrically active donors for the same location of the Fermi energy relative to E_{FS}. The calculated n_{max} as a function of x for $Ga_{1-3x}In_{3x}N_xAs_{1-x}$ only considering the downward shift of the conduction band caused by the band anticrossing, as well as that also including the increase in the effective mass can be obtained using[81]

$$n(E_F) = \int \frac{\rho(E)\, dE}{1 + \exp[(E - E_F)/k_B T]}, \quad (3)$$

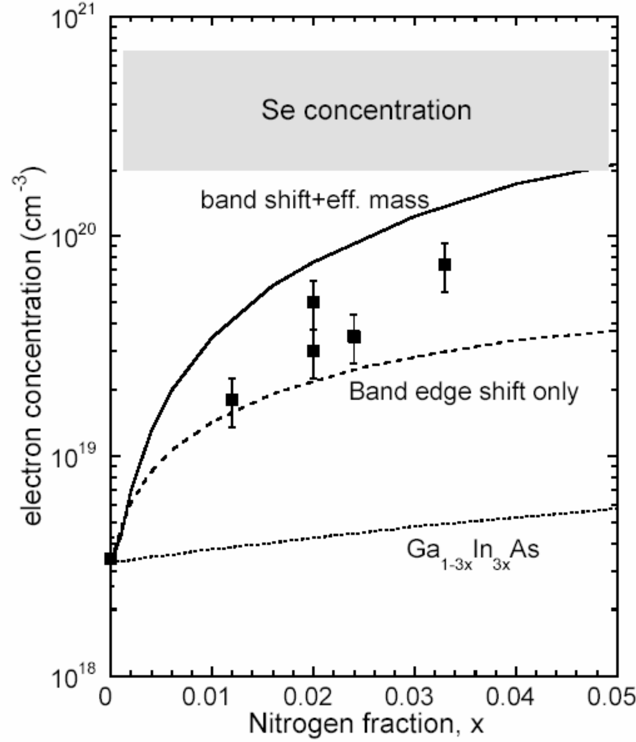

Figure 6. Comparison of the measured maximum electron concentration with the calculated values as a function of N fraction in $Ga_{1-3x}In_{3x}N_xAs_{1-x}$. Two different cases of the calculated n_{max} are shown: one includes effects of downward shift of the conduction band only (dashed curve) and the other includes both the band shift and the enhancement of the density of states (solid curve). The calculated n_{max} for samples without N (*i.e.* when only the effects from the band-gap lowering produced by In incorporation are considered) are also shown (dotted curve) for comparison. The shaded area indicates the range of Se concentration in these samples.

where $\rho(E)$ is the perturbed density of states. The results are shown in Fig. 6. Comparison of the experimental data with the calculation shows that in order to account for the large enhancement of the doping limits in III-N-V alloys both effects, the downward shift of the conduction band and the increase of the effective mass have to be taken into account.

While Se doped $Ga_{1-3x}In_{3x}N_xAs_{1-x}$ alloys grown by MOCVD have shown enhanced n_{max} in accordance with the BAC model, similar

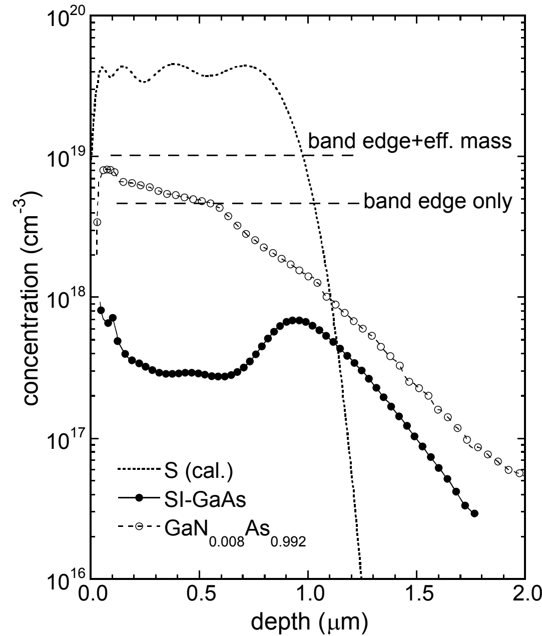

Figure 7. Ionized net donor concentration profiles for the GaN_xAs_{1-x} films and the SI-GaAs standard measured by the electrochemical capacitance-voltage (ECV) technique. The short-dashed curve is the calculated distribution of implanted S atoms. The dashed horizontal lines indicate the theoretical free electron concentrations in $Ga_{1-x}N_xAs$ by considering only the effects of the downward shift of the conduction band (band edge only) and both the effects of band-gap reduction and density of states effective mass enhancement (band edge + effective mass).

behavior is also observed in S^+-implanted GaN_xAs_{1-x} thin films.[82] Figure 7 displays the carrier concentration profiles measured by the ECV technique for S implanted GaN_xAs_{1-x} (x~0.008) and SI-GaAs samples after RTA. A striking difference in the free electron concentration n measured in the SI-GaAs and the GaN_xAs_{1-x} samples is observed. In the S^+-implanted SI-GaAs sample, $n \sim 2.5\times10^{17}$cm^{-3} was measured in the bulk of the implanted layer, with a higher $n \sim 5\times10^{17}$cm^{-3} towards the end of the implantation profile. The theoretical n_{max} in GaN_xAs_{1-x} due to the N-induced conduction band modification within the framework of the

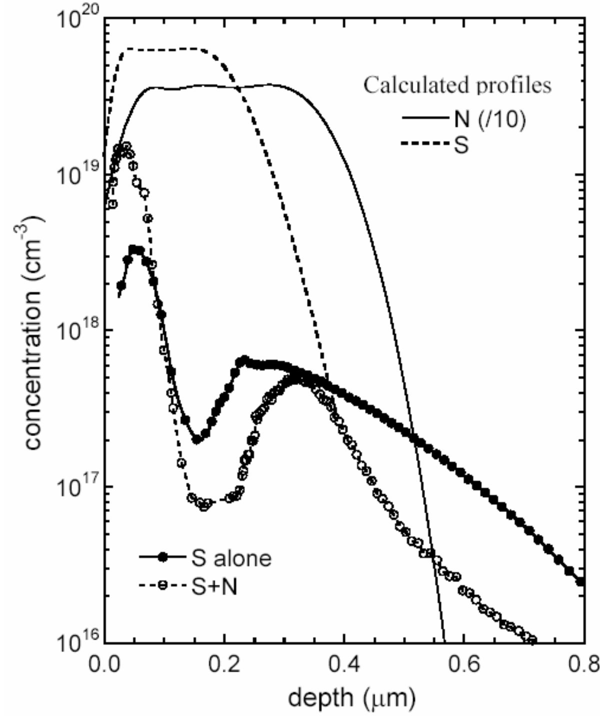

Figure 8. The ECV measured net donor concentration profiles for the GaAs samples implanted with S alone and S+N after RTA at 945°C for 10s. The calculated atomic profiles for both the implanted S and N are also shown.

BAC model and the amphoteric native defect model is ~1×10^{19} cm^{-3} for the $GaN_{0.008}As_{0.992}$ sample. This value is in a reasonably good agreement with the measured concentration of 6×10^{18} cm^{-3} shown in Fig. 7.

Attempts to form n-type GaN_xAs_{1-x} thin films with high electron concentration were also made by co-implantation of N and a dopant element in GaAs.[83] Figure 8 shows a comparison of the ECV determined free electron concentration profiles for GaAs samples implanted with S alone and co-implanted with S and N (S+N) after RTA at 945°C for 10s. The calculated as-implanted S and N atomic distributions are also shown in the figure. The most prominent difference in the electron concentration profiles between the S only and (S+N) samples is the much enhanced electron concentration in the (S+N) sample in a narrow region

(~500Å) near the surface. The region with lower electron concentration at ~0.1-0.2 μm below the surface coincides with a region with excess As due to the implantation process that makes the substitution of S atoms into the As sites more difficult.[84] In addition, larger concentrations of the compensating V_{Ga} acceptors are also expected in the As-rich region. A reduced availability of group V sites and an increased V_{Ga} concentration in the region lead to the minimum in the electron concentration. The effect is exacerbated in the (S+N) sample where both S and N compete for the same group V element sites.

Considering both band gap reduction and large increase in the electron effective mass, the high n_{max} in the near-surface region of the (S+N) sample ($\sim 1.5\times10^{19}cm^{-3}$) implies that the N content in this thin near-surface diluted nitride layer is x=0.0032. This value is in good agreement with the calculated N concentration in the surface region (x≈0.003-0.01). With this N content the conduction band edge is shifted downward by 77 meV and the conduction band effective mass at the Fermi energy becomes about three times larger than that of GaAs.[84]

5. Concluding Remarks: *From Dilute III-N-V Nitrides to Dilute II-O-VI Oxides*

Although this chapter has been devoted to III-N-V alloys, we would like to conclude it by pointing out that the experimental and theoretical methods developed for the dilute nitrides should be generally applicable to other semiconductor alloys with isoelectronic substitution of elements with highly mismatched electronegativities.

It has been demonstrated that group II-O-VI alloys in which highly electronegative O partially replaces the group VI element show a modification of the electronic similar to that found in III-N-V alloys. For example, a dramatic O-induced reduction of the bandgap has been reported in $Cd_{1-y}Mn_yO_xTe_{1-x}$ and ZnO_xSe_{1-x}.[85,86] Thus, partial replacement of group-VI anions with more electronegative O atoms in II-VI compounds does have the effect similar to incorporating nitrogen into III-V materials. It has been shown that the electronic structure of these alloys can be well described by that BAC model.

The O-induced modification of the conduction band structure of II-VI compound semiconductors offers an interesting possibility of using small amounts of O to engineer the optoelectronic properties of group II-O-VI alloys. One important technological potential of dilute oxides is for photovoltaic solar energy conversion. Efforts to improve the

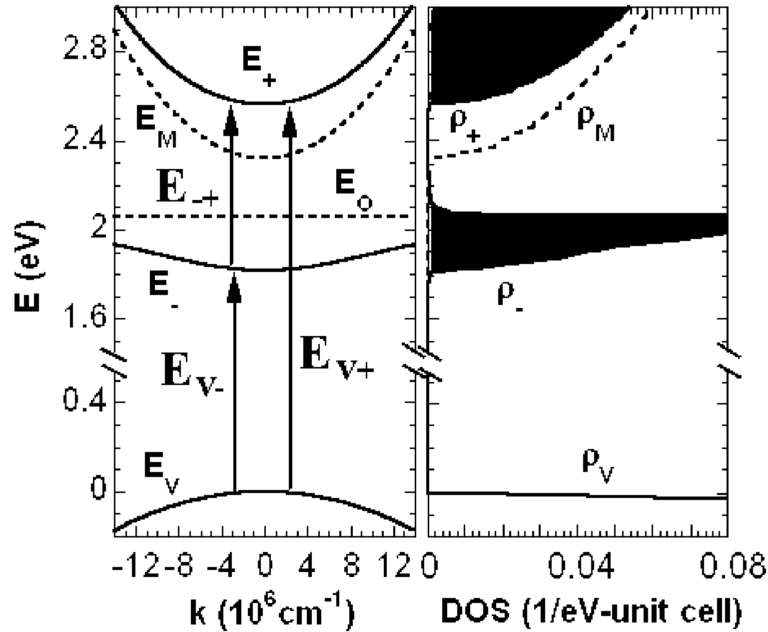

Figure 9. The calculated energy band structure (left panel) and density of states (right panel) for $Zn_{0.88}Mn_{0.12}O_xTe_{1-x}$ with x~0.01. The three possible optical transitions are indicated in the left panel.

efficiency of solar cells have led to extensive experimental and theoretical studies of new materials and cell designs. To date, the highest power conversion efficiency of ~37% has been achieved with multi-junction solar cells based on standard semiconductor materials.[29,87,88] It was recognized over thirty years ago that the introduction of states in a semiconductor band gap presents an alternative to multi-junction designs for improving the power conversion efficiency of solar cells.[89-91] It was argued that deep impurity or defect states could play the role of the intermediate states for this purpose. Detailed theoretical calculations indicate that a single junction cell with one or two properly located bands of intermediate states could achieve power conversion efficiencies up to 62% (Ref.90) and 71.7% (Ref.91), respectively. However, difficulties in controlling the incorporation of high concentrations of impurity or defect states have hindered prior efforts to realize such materials.

It has been recently found that, with the multiple band gaps that fall within the solar energy spectrum, $Zn_{1-y}Mn_yO_xTe_{1-x}$ provides a unique opportunity for the realization of the proposed multiband solar cell.[92,93] The energy band structure and the density of states for the case of $Zn_{0.88}Mn_{0.12}O_xTe_{1-x}$ alloy (with x~0.03) are shown in Fig. 9. An O derived narrow band of extended states $E_$ is separated from the upper subband E_+ by about 0.7 eV. Three types of optical transitions are possible in this band structure: (1) from the valence band to the E_+ subband, $E_{V+}=E_+(k=0)-E_V(k=0)=2.56$ eV, (2) from the valence band to $E_$ subband, $E_{V_}=E_(k=0)-E_V(k=0)=1.83$ eV, and (3) from $E_$ to E_+, $E_{+_}=E_+(k=0)-E_(k=0)=0.73$ eV. These three absorption edges span much of the solar spectrum, indicating that dilute oxide II-O-VI alloys could be good candidates for the multi-band semiconductors envisioned for high efficiency photovoltaic devices. Solar cells made from such a three-band material have a number of advantages over multi-junction solar cells that include much simpler device structure and much lower cost, as well as higher solar energy conversion efficiency.

Acknowledgements

This work was supported by the Director, Office of Science, Office of Basic Energy Sciences, Division of Materials Sciences and Engineering, of the U.S. Department of Energy under Contract No. DE-AC03-76SF00098.

References

1. M. Weyers, M. Sato, H. Ando, Jpn. J. Appl. Phys. **31**, L853 (1992).
2. M. Kondow, K. Uomi, K. Hosomi and T. Mozume, Jpn. J. Appl. Phys. **33**, L1056 (1994).
3. C. Skierbiszewski, P. Perlin, P. Wisniewski, W. Knap, T. Suski, W. Walukiewicz, W. Shan, K.M. Yu, J.W. Ager, E.E. Haller, J.F. Geisz, and J.M. Olson, Appl. Phys. Lett. **76**, 2409(2000).
4. J.F. Geisz, D.J. Friedman, J.M. Olson, S.R. Kurtz, and M.B. Keyes, J. Cryst. Growth, **195**, 401(1998).
5. S.R. Kurtz, Allerman, C.H. Seager, R.M. Sieg, and E.D. Jones, Appl. Phys. Lett. **77**, 400(2000).
6. W. Shan, W. Walukiewicz, J. W. Ager III, E. E. Haller, J. F. Geisz, D. J. Friedman, J. M. Olson, and S. R. Kurtz, Phys. Rev. Lett. **82**, 1221(1999).
7. J. D. Perkins, A. Masceranhas, Y. Zhang, J. F. Geisz, D. J. Friedman, J. M. Olson, and S. R. Kurtz, Phys. Rev. Lett. **82**, 3312(1999).
8. K. Uesugi, N. Marooka, and I. Suemune, Appl. Phys. Lett. **74**, 1254(1999).

9. J.A. Van Vechten, T.K.Bergstresser, Phys. Rev. B**1**, 3351 (1970).
10. D. Richardson, J. Phys. C: Solid State Phys. **4**, L289 (1971).
11. H.C. Casey, M.B. Panish, J. Appl. Phys. **40**, 4910 (1969).
12. J. N. Baillargeon, K. Y. Cheng, G. E. Hofler, P. J. Pearah and K. C. Hsieh, Appl. Phys. Lett. **60**, 2540(1992).
13. M. Kondow, K. Uomi, K. Hosomi, and T. Mozume, Jpn. J. Appl. Phys. Part 2, **33**, L1056 (1994).
14. W.G. Bi, and C.W. Tu, J. Appl. Phys. **80**, 1934 (1996).
15. M. Kondow, T. Kitatani, S. Nakatsuka, M.C. Larson, K. Nakahara, Y. Yazawa, M. Okai, K. Uomi, IEEE J. Sel. Topic in Quantum Electronics, **3**, 719 (1997).
16. See, for example, *Dilute Nitride (III-N-V) Semiconductors: Physics and Technology*, ed. M. Henini, Elsevier, London, 2004, Chpts. 1-4.
17. See, for example, J.S. Harris Jr, Semicond. Sci. Technol, **17**, 880 (2002), and references there in.
18. M. Kondow, K. Uomi, A. Niwa, T. Kitatani, S. Watahiki, and Y. Yazawa, Jpn. J. Appl. Phys. **35**, 1273 (1996).
19. T. Miyamoto, T. Kageyama, S. Makino, D. Schlenker, F. Koyama and K. Iga, J. Cryst. Growth, **209**, 339 (2000).
20. W. Shan, K.M. Yu, W. Walukiewicz, J.W. Ager III, E.E. Haller, M.C. Ridgway, Appl. Phys. Lett. **75**, 1410(1999).
21. K.M. Yu, W. Walukiewicz, J. Wu, J. Beeman, J.W. Ager III, E.E. Haller, W. Shan, H.P. Xin, C.W. Tu, M.C. Ridgway. Appl. Phys. Lett. **78**, 1077(2001); J. Appl. Phys. **90**, 2227(2001).
22. J. Jasinski, K.M. Yu, W. Walukiewicz, Z. Liliental-Weber, J. Washburn, Appl. Phys. Lett. **79**, 931(2001).
23. K.M. Yu, W. Walukiewicz, M.A. Scarpulla, O.D. Dubon, J. Jasinski, Z. Liliental-Weber, J. Wu, J. Beeman, M.R. Pillai, M.J. Aziz, J. Appl. Phys. **94**, 1043(2003).
24. K.M. Yu, W. Walukiewicz, J. Wu, W. Shan, J. Beeman, M.A. Scarpulla, O.D. Dubon, M.C. Ridgway, D.E. Mars, D.R. Chamberlin, Appl. Phys. Lett. **83**, 2844(2003).
25. C.W. White, P.S. Percy, *Laser and Electron Beam Processing of Materials*, Academic Press, (New York 1980).
26. J.S. Williams, *Laser Annealing of Semiconductors*. Ed. J.M. Poate and J.M. Mayer, Academic Press, (New York, 1982), p.385.
27. J.M. Olson, S.R. Kurtz, A.E. Kibbler, and P. Faine, *Appl. Phys. Lett.* **56**, 623 (1990).
28. R.R. King, *et al. Proc. 28th IEEE Photovoltaic Specialists Conference,* (New York: IEEE, 2000) p 998.
29. H.L. Cotal *et al*. *Proc. 28th IEEE Photovoltaic Specialists Conference,* (New York: IEEE, 2000) p 955.
30. S.R. Kurtz, D. Myers, and J.M. Olson, *Proc. 26th IEEE Photovoltaic Specialists Conference,* (New York: IEEE, 1997) p 875.
31. D.J. Friedman, J.F. Geisz, S.R. Kurtz, and J.M. Olson, J. Cryst. Growth*,* **195**, 409 (1998).
32. H.Q. Hou, K.C. Reinhardt, S.R. Kurtz, J.M. Gee, A.A. Allerman, B.E. Hammons, P.C. Chang, and E.D. Jones, *Proc. 2nd World Conf. on Photovoltaic Energy Conversion* (Piscataway, NJ: IEEE, 1998) p.3600.
33. D.J. Friedman, J.F. Geisz, S.R. Kurtz, and J.M. Olson, *Proc. 2nd World Conf. on Photovoltaic Energy Conversion,* (Piscataway, NJ: IEEE, 1998) p.3.

34. S.R. Kurtz, A.A. Allerman, E.D. Jones, J.M. Gee, J.J. Banas, and B.E. Hammons, Appl. Phys. Lett. **74**, 729 (1999).
35. S.R. Kurtz, A.A. Allerman, C.H. Seager, R.M. Sieg, and E.D. Jones, Appl. Phys. Lett. **77**, 400 (2000).
36. S.R. Kurtz, J.F. Geisz, D.J. Friedman, J.M. Olson, A. Duda, N.H. Karam, R.R. King, J.H. Ermer, and D.E. Joslin, *Proc. 28th IEEE Photovoltaic Specialists Conference,* (New York: IEEE, 2000) p 1210.
37. S.R. Kurtz, J.F. Klem, A.A. Allerman, R.M. Sieg, C.H. Seager, and E.D. Jones, Appl. Phys. Lett. **80**, 1379 (2002).
38. J.C. Phillips, *Bonds and Bands in Semiconductors*, Academic, New York, 1973, p.54.
39. S. Sakai, Y. Ueta, and Y. Terauchi, Jpn. J. Appl. Phys. Part 1, **32**, 4413 (1993).
40. G. Pozina, I. Ivanov, B. Monemar, J. V. Thordson, and T. G. Andersson, J. Appl. Phys. **84**, 3830 (1998).
41. J. Sik, M. Schubert, G. Leibiger, V. Gottschalch, G. Kirpal, and J. Humlicek, Appl. Phys. Lett. **76**, 2859 (2000).
42. A. Ougazzaden, Y. Le Bellego, E. V. K. Rao, M. Juhel, L. Leprince, and G. Patriarche, Appl. Phys. Lett. **70**, 2861 (1997).
43. T. Makimoto, H. Saito, T. Nishida, and N. Kobayashi, Appl. Phys. Lett. **70**, 2984 (1997).
44. M. Kozhevnikov, V. Narayanamurti, C. V. Reddy, H. P. Xin, C. W. Tu, A. Mascarenhas, and Y. Zhang, Phys. Rev. B **61**, R7861 (2000).
45. S.-H. Wei and A. Zunger, Phys. Rev. Lett. **76**, 664 (1996).
46. J. Neugebauer and C. G. Van de Walle, Phys. Rev. B **51**, 10568 (1995).
47. A. Rubio and M. L. Cohen, Phys. Rev. B **51**, 4343 (1995).
48. L. Bellaiche, S.-H. Wei, and A. Zunger, Phys. Rev. B **54**, 17568 (1996).
49. L. Bellaiche, S.-H. Wei, and A. Zunger, Appl. Phys. Lett. **70**, 3558 (1997).
50. T. Mattila, S.-H. Wei, and A. Zunger, Phys. Rev. B **60**, R11245 (1999).
51. H.P. Hjalmarson, P. Vogl, D.J. Wolford, J.D. Dow, Phys. Rev. Lett. **44**, 810 (1980).
52. D.J. Wolford, J.A. Bradley, K. Fry, J. Thompson, in *Physics of Semicondutors*, ed. J.D. Chadi and W.A. Harrison (Springer, New York, 1984), p.627.
53. X. Liu, S.G. Bishop, J.N. Baillargeon, and K.Y. Cheng, Appl. Phys. Lett. **63**, 208 (1993).
54. Y. Makita, H. Ijuin, and S. Gonda, Appl. Phys. Lett. **28**, 287 (1976).
55. E. D. Jones, N. A. Modine, A. A. Allerman, S. R. Kurtz, A. F. Wright, S. T. Tozer, and X. Wei, Phys. Rev. B **60**, 4430 (1999).
56. W. Walukiewicz, W. Shan, J. W. Ager III, D. R. Chamberlin, E. E. Haller, J. F. Geisz, D. J. Friedman, J. M. Olson, and S. R. Kurtz, in *Photovoltaics for the 21st Century*, ed. V.K. Kapur, R.D. McDonnell, D. Carlson, G.P. Ceasar, and A. Rohatgi, (The Electrochemical Society, Pennington, NJ, 1999), p.199.
57. J. Endicott, A. Patanè, J. Ibáñez, L. Eaves, and M. Bissiri, M. Hopkinson, R. Airey, and G. Hill, Phys Rev. Lett. **91**, 126802 (2003).
58. A. Lindsay and E. P. O'Reilly, Solid State Commun. **112**, 443 (1999).
59. E. P. O'Reilly and A. Lindsay, Phys. Status Solidi (b), **216**, 131 (1999).
60. E.P. O'Reilly, A. Lindsay, S. Tomic, and M. Kamal-Saadi, Semicond. Sci. Technol. **17**, 870(2002).
61. S. A. Choulis, S. Tomic, E. P. O'Reilly, and T. J. C. Hosea, Solid State Commun. **125**, 155 (2003).

62. S. A. Choulis, T. J. C. Hosea, S. Tomic, M. Kamal-Saadi, A. R. Adams, E. P. O'Reilly, B. A. Weinstein, and P. J. Klar, Phys. Rev. B **66**, 165321 (2002).
63. B. Gil, Solid State Commun. **114**, 623 (2000).
64. N. Shtinkov, P. Desjardins, and R. A. Masut, Phys. Rev. B **67**, 081202 (2003).
65. P.J. Klar, H. Gruning, J. Koch, S. Schafer, K. Volz, W. Stolz, W. Heimbrodt, A.M. Kamal-Saadi, A. Lindsay, and E.P. O'Reilly, Phys. Rev. B **64**, 121203 (2001).
66. P.J. Klar, H. Gruning, W. Heimbrodt, G. Weiser, J. Koch, S. Schafer, K. Volz, W. Stolz, S.W. Koch, S. Tomic, S.A. Chouli, T.J.C. Hosea, E.P. O'Reilly, M. Hofmann, J. Hader, and J.V. Moloney, Semicond. Sci. Technol, **17**, 830 (2002).
67. P. R. C. Kent and A. Zunger, Phys. Rev. Lett. **86**, 2613 (2001); Phys. Rev. B **64**, 115208 (2001).
68. G. Szwacki and P. Boguslawski, Phys. Rev. B **64**, 161201 (2001).
69. I. Vurgaftman and J.R. Meyer, J. Appl. Phys. **94**, 3675 (2003).
70. A. Lindsay, S. Tomic, and E. P. O'Reilly, Solid-State Electron. **47**, 443 (2003).
71. R. Bhat, C. Caneau, L. Salamanca-Riba, W.G. Bi, C.W. Tu, J. Crystl. Growth, **195**, 427 (1998);
72. L. Malikova, F.H. Pollak, R. Bhat, J. Electron. Mat. **27**, 484 (1998);
73. B.M. Keyes, J.F. Geisz, P.C. Dippo, R. Reedy, C. Kramer, D.J. Friedman, S.R. Kurtz, J.M. Olson, AIP Conf. Proc. **462**, 511 (1999).
74. W. Shan, W. Walukiewicz, J.W. Ager III, E.E. Haller, J.F. Geisz, D.J. Friedman, J.M. Olson, and S.R. Kurtz, J. Appl. Phys. **86**, 2349 (1999).
75. P.J. Klar, H. Grüning, W. Heimbrodt, J. Koch, F. Höhnsdorf, W. Stolz, P.M.A. Vicente, and J. Camassel, Appl. Phys. Lett. **76**, 3439 (2000).
76. C Skierbiszewski, Semicond. Sci. Technol. **17**, 803 (2002).
77. W. Walukiewicz, Appl. Phys. Lett. **54**, 2094 (1989); Mat. Res. Soc. Symp. Proc. **300**, 421 (1993).
78. S.B. Zhang, S.H. Wei, A. Zunger. J. Appl. Phys. **83**, 3192 (1998).
79. W. Walukiewicz, Mats. Science Forum, Vols.**143-147**, 519 (1993).
80. K.M. Yu, W. Walukiewicz, W. Shan, J.W. Ager III, J. Wu, E.E. Haller, J.F. Geisz, D.J. Friedman, J.M. Olson. Phys. Rev. B **61**, R13337 (2000).
81. J. Wu, W. Shan, W. Walukiewicz, Semicond. Sci. Technol. **17**, 860 (2002).
82. K.M. Yu, W. Walukiewicz, W. Shan, J. Wu, J.W. Ager III, E.E. Haller, J.F. Geisz, M.C. Ridgway, Appl. Phys. Lett. **77**, 2858 (2000).
83. K.M. Yu, W. Walukiewicz, W. Shan, J. Wu, J. Beeman, J.W. Ager III, E.E. Haller. App. Phys. Lett. **77,** 3607 (2000).
84. C. Skierbiszewski, P. Perlin, P. Wišniewski, W. Knap, T. Suski, W. Walukiewicz, W. Shan, K.M. Yu, J.W. Ager III, E.E. Haller, J.F. Geisz, J.M. Olson. Appl. Phys. Lett. **76**, 2409 (2000).
85. K.M.Yu, W.Walukiewicz, J.Wu, J.W. Beeman, J.W. Ager, E. E. Haller, I. Miotkowski, A. K. Ramdas, and P. Becla, Appl. Phys. Lett. **80**, 1571 (2002).
86. W. Shan, W. Walukiewicz, J.W. Ager III, K.M. Yu, J. Wu, E.E. Haller, Y. Nabetani, T. Mukawa, Y. Ito, T. Matsumoto, Appl. Phys. Lett. **83**, 299 (2003).
87. P.K. Chiang, J.H. Ermer, W.T. Nishikawa, D.D. Krut, D.E. Joslin, J.W. Eldredge, B.T. Cavicchi, and J.M. Olson, *Proc. 25th IEEE Photovoltaic Specialists Conf.* (IEEE New York, 1996) p. 183.
88. R.R. King, P.C. Colter, D.E. Joslin, K.M. Edmondson, D.D. Krut, N.H. Karam, and Sarah Kurtz, *Proc. 29th IEEE Photovoltaic Specialists Conf.* New Orleans, (IEEE, New York, 2002) p. 852.

89. M. Wolf, Proc. IRE, **48**, 1246(1960).
90. A. Luque and A. Marti, Phys. Rev. Lett. **78**, 5014 (1997).
91. A. S. Brown, M. A. Green and R. P. Corkish, Physica, E**14**, 121 (2002).
92. K. M. Yu, W. Walukiewicz, J. Wu, W. Shan, J. W. Beeman, M. A. Scarpulla, O. D. Dubon, and P. Becla, Phys. Rev. Lett. **91**, 246203 (2003).
93. W. Shan, W. Walukiewicz, K.M. Yu, J.W. Ager III, J. Wu, J. Beeman, M.A. Scapulla, O.D. Dubon, E. E. Haller, Y. Nabetani, and P. Becla, SPIE Proc. Vol.**5349**, 426 (2004).